Soft Matter

ROYAL SOCIETY OF CHEMISTRY

PAPER

View Article Online
View Journal | View Issue

Cite this: *Soft Matter*, 2026, **22**, 692

Preparation of functional Zein/*Spirulina* protein isolate nanocomposite particles for improved encapsulation of glabridin

Jie Mei,[a] Chen Li,[b] Beizhe Chang,[a] Xiaomin Li,[a] Yunxing Li,[a]* Bingtian Zhao,[a] Cheng Yang*[a] and To Ngai[c]*

Received 19th September 2025,
Accepted 10th December 2025

DOI: 10.1039/d5sm00953g

rsc.li/soft-matter-journal

This study reports the possibility of employing Zein/*Spirulina* protein isolate (Zein/SPI) nanocomposite particles as a functional carrier for lipophilic bioactives, using glabridin (GLA) as a model. Zein/SPI nanocomposite particles are synthesized using a conventional anti-solvent precipitation process. The combination of zein and SPI occurs because of electrostatic attraction, hydrophobic interaction, and hydrogen bonding. With an optimal Zein/SPI weight ratio, high encapsulation efficiency and loading capacity of GLA are attained with Zein/SPI nanocomposite particles. GLA is successfully encapsulated in an amorphous form. The presence of SPI improves nanoparticle resilience to aggregation and sedimentation under different environmental conditions. Compared to free GLA, encapsulation enhances GLA stability against ultraviolet light, thermal treatment, and long-term storage. Encapsulated GLA also demonstrates better antioxidant activity than GLA dispersed in water. Additionally, a cytotoxicity study reveals that Zein/SPI nanocomposite particles are highly biocompatible. The *in vitro* release profile shows a steady and slow release of encapsulated GLA without a burst effect. These results suggest that Zein/SPI nanocomposite particles can be used as all-natural carriers for lipophilic and unstable bioactives in food, pharmaceuticals, and cosmetics.

1. Introduction

Glabridin (GLA), a natural flavonoid compound with diverse beneficial properties, including anti-inflammatory, antioxidant, and anticancer properties, has received significant attention for its potential to improve human health and prevent disease.[1,2] However, poor water solubility and low stability severely restrict its practical applications.[3,4] Encapsulating strategies have been extensively investigated as effective ways to improve the solubility and stability of hydrophobic bioactives.[5,6] Furthermore, encapsulation allows for controlled release of bioactives, which improves their efficacy and safety. Nanoparticles have emerged as a promising carrier for the encapsulation of bioactives because of their small size, large surface area, and controllable surface properties.[7] Nanoparticles protect against environmental stress, allow for slow, sustained and targeted release, and improve cellular uptake and intracellular transport of bioactives, making them ideal for use in the food, pharmaceutical, and cosmetic industries.[8,9]

Zein, a corn-derived plant protein, has attracted extensive interest as a nanoparticle-forming material due to its inherent amphiphilicity, biodegradability, and biocompatibility.[10–13] Zein nanoparticles (ZNPs) have been shown to effectively encapsulate, protect, and controllably release a variety of hydrophobic compounds.[14–18] Nonetheless, their practical applications are hampered by poor colloidal stability, especially at physiological pH and high ionic strength, where particle aggregation and precipitation occur frequently. To address these constraints, several stabilizers, including polysaccharides, proteins, and surfactants, have been studied.[19,20] However, the majority of current research focuses on improving particle stability, with relatively few efforts going toward endowing ZNPs with additional function. This represents a significant gap and an attractive opportunity to exploit novel materials that not only stabilize ZNPs but also provide additional functionalities.

Spirulina protein isolate (SPI), derived from *Spirulina platensis*, has great potential as a functional component in nanoparticle production.[21,22] It possesses excellent protein-surface-related properties including emulsifying, foaming, and gel-forming properties, along with inherent bioactivities such as

[a] *Key Laboratory of Synthetic and Biological Colloids, Ministry of Education, School of Chemical and Material Engineering, Jiangnan University, Wuxi, 214122, China. E-mail: yunxingli@jiangnan.edu.cn, cyang@jiangnan.edu.cn*
[b] *School of Chemistry, Biology and Environment, Yuxi Normal University, Yuxi, 653100, China*
[c] *Department of Chemistry, The Chinese University of Hong Kong, Shatin, N. T., Hong Kong, China. E-mail: tongai@cuhk.edu.hk*

antioxidant and anti-inflammatory properties, and the ability to absorb ultraviolet light.[23–25] These distinguishing characteristics make SPI especially appealing as a stabilizer for improving the stability and performance of zein-based nanoparticles. Despite its potential, the use of SPI with zein to design and fabricate nanocomposite particles has yet to be investigated.

In this study, SPI was used as a novel stabilizer to improve the colloidal stability and functionality of ZNPs. Zein/SPI nanocomposite particles were fabricated *via* an antisolvent precipitation method, and their potential as carriers of hydrophobic substances was tested using GLA as a model compound. The influence of the Zein/SPI mass ratios on the formation of Zein/SPI nanocomposite particles and the interactions between zein and SPI were initially explored. Following the introduction of GLA into the anti-solvent process, the encapsulation efficiency and loading capacity of GLA, as well as the formation and colloidal stability of GLA-loaded Zein/SPI nanocomposite particles, were investigated further. Finally, the stability, bioactivity, cytotoxicity and release behavior of free and encapsulated GLA were compared.

2. Experimental

2.1 Materials

Zein (Z3625) was obtained from Sigma-Aldrich (Shanghai, China). *Spirulina* powder and glabridin were purchased from Guangyu Biological Technology Co., Ltd (Shanghai, China) and Yuanye Bio-Technology Co., Ltd (Shanghai, China), respectively. Ethanol, HCl, NaCl, NaOH, KBr, $FeCl_3$, sodium acetate, ascorbic acid, sodium dodecyl sulfate (SDS), Na_2HPO_4, NaH_2PO_4, and $K_2S_2O_8$ were supplied by Sinopharm (Shanghai, China). Ethanol (HPLC grade), acetic acid (HPLC grade), DL-1,4-dithiothreitol (DTT, ≥99%), 2,4,6-tri(pyridin-2-yl)-1,3,5-triazine (TPTZ), urea and Tween-80 were purchased from Titan Scientific Co., Ltd (Shanghai, China). Isosorbide dimethyl ether (98%) was bought from Macklin Biochemical Technology Co., Ltd (Shanghai, China). HaCaT cells (human immortalized epidermal cells, BNCC339817) and NCM-460 cells (human normal colonic epithelial cells, BNCC339288) were supplied by BeNa Culture Collection (Beijing, China). 2,2′-Azino-bis (3-ethylbenzothiazoline-6-sulfonic acid) diammonium salt (ABTS) and Cell Counting Kit-8 (CCK-8) were supplied by Meryer Biochemical Technology Co., Ltd and Beyotime Biotechnology (Shanghai, China), respectively. Phosphate buffered saline (PBS) and Dulbecco's modified Eagle medium (DMEM) were supplied by Cytiva (Shanghai, China) and Gibco (Suzhou, China), respectively.

2.2 Preparation of zein-based nanoparticles and those loaded with glabridin

Zein powder (100 mg) was dissolved in aqueous ethanol (20 mL, 80 vol%) to prepare a stock solution. The SPI was isolated from *Spirulina* powder using the method reported by Ding *et al.*[21] Different quantities of SPI (25, 50, 75, 100, and 150 mg) were dissolved in deionized water (100 mL) and then, the pH of the resulting solutions was adjusted to 5.0. Under magnetic stirring, zein stock solution (20 mL) was quickly added to the above SPI solution. After several minutes of stirring, the ethanol was removed using rotary evaporation (35 °C, −0.1 MPa). The resulting dispersion was then made up with water to 100 mL. The appreciable aggregates were removed by centrifugation (1000 rpm) for 10 min. The prepared Zein/SPI nanocomposite particles with Zein/SPI mass ratios of 1 : 0.25, 1 : 0.5, 1 : 0.75, 1 : 1, and 1 : 1.5 were designated as Zein/$SPI_{1:0.25}$, Zein/$SPI_{1:0.5}$, Zein/$SPI_{1:0.75}$, Zein/$SPI_{1:1}$, and Zein/$SPI_{1:1.5}$, respectively. The above procedure was used to generate a dispersion of ZNPs by replacing the SPI solution with pH 5.0 deionized water.

To prepare GLA-loaded Zein/SPI nanocomposite particles (ZSG), a specific amount (5, 10, 15, 20, or 25 mg) of GLA was initially dissolved in the as-prepared zein stock solution (20 mL) under ultrasonication. The following process was the same as the fabrication of Zein/SPI nanocomposite particles. The resulting ZSG was classified as ZSG_5, ZSG_{10}, ZSG_{15}, ZSG_{20}, and ZSG_{25}, respectively. In the preparation of GLA-loaded ZNPs (ZG), the SPI solution was replaced with pH 5.0 deionized water, but the rest of the method remained unchanged. The ZG corresponding to GLA of 5, 10, 15, 20, and 25 mg were designated ZG_5, ZG_{10}, ZG_{15}, ZG_{20}, and ZG_{25}, respectively.

2.3 Characterization of nanoparticles

2.3.1 Dynamic light scattering (DLS). The samples were adequately diluted with deionized water (pH 5.0) to prevent multiple scattering while still obtaining a significant enough signal to measure. The size distribution, polydispersity index (PDI), and zeta potential were detected using the NanoBrook Omni Series analyzer (Brookhaven, USA). All measurements were taken at 25 °C and in triplicate.

2.3.2 Scanning electron microscopy (SEM). The samples were robustly immobilized on a double-sided conductive tape and sputter-coated with a gold overlayer. Morphological observations were conducted using an S-4800 electron microscope (Hitachi, Japan) at an accelerating voltage of 3 kV.

2.3.3 Fourier transform infrared (FTIR) spectroscopy. Freeze-dried sample was combined with KBr powder and pressed into a pellet using a tablet press. FTIR spectra were collected using the Nicolet iS5 spectrometer (Thermo Fisher Scientific, USA) over a range of 500 to 4000 cm^{-1} with a resolution of 4 cm^{-1}.

2.3.4 Ultraviolet-visible (UV-vis) spectroscopy. A PERSEE TU1950 spectrophotometer (Beijing, China) was employed to analyse the characteristic absorption. Before taking measurements, the sample was diluted to an acceptable concentration in deionized water with a pH of 5.

2.3.5 Fluorescence spectroscopy. A triangle quartz cuvette was filled with the solution or dispersion of samples after they had been suitably diluted with deionized water at a pH of 5.0. Fluorescence spectra were recorded at room temperature using a spectrophotometer (Hitachi F-7000, Japan). With a given excitation wavelength (280 nm), spectra were obtained across the emission wavelength range of 290 to 450 nm. Slit widths of

excitation/emission and scanning speed were set to 5 nm and 1200 nm min^{-1}, respectively.

2.3.6 X-ray diffraction (XRD). Freeze-dried samples were homogenously distributed in a sample slot, and the surface was gently flattened with a glass slide and analysed using an AXS D8 Advance diffractometer (Bruker, Germany). XRD measuring settings include a scanning angle (2θ) of 5 to 55° and a speed of 5° min^{-1}. A copper anode was employed, the current and voltage were set to 40 mA and 40 kV, respectively.

2.3.7 Differential scanning calorimetry (DSC). The freeze-dried powders underwent thermal analysis using a DSC 8000 differential scanning calorimeter (PerkinElmer, UK), with about 5 mg of sample. The instrument parameters were set as follows: a scanning temperature range of 30 to 150 °C, a heating rate of 10 °C min^{-1}, and a nitrogen flow rate of 20 mL min^{-1}.

2.4 Driving force analysis

Sodium dodecyl sulfate (SDS), urea and DL-1,4-dithiothreitol (DTT) were used to determine the hydrophobic interaction, hydrogen bonding, and disulfide bonding between zein and SPI.[26] Mixtures were prepared by vortexing the aqueous dispersion of Zein/$SPI_{1:1}$ with equal-volume solutions of SDS, urea, or DTT at various concentrations for 10 s, followed by leaving them undisturbed for 6 h in a dark environment. Next, a microplate reader was used to determine the absorbance of these samples at 600 nm, which was defined as the turbidity of the sample. The absorbance of the samples was compared with Zein/$SPI_{1:1}$ which was mixed with an equal volume of water. Any changes in the absorbance directly reflect the driving force between zein and SPI.

2.5 Encapsulation efficiency (EE) and loading capacity (LC) of GLA

200 μL ZSG or ZG aqueous dispersion was mixed with ethanol (1.8 mL), sonicated for 30 min and then vortexed to dissolve the carrier particles and release the GLA. HPLC was employed to analyze the GLA released after filtering the fluid across a membrane (pore size, 0.22 μm). A Waters Arc HPLC system (USA) was used, fitted with a symmetry C18 column (4.6 × 250 mm, 5 μm). The mobile phase comprised ethanol and 0.5% (w/w) acetic acid solution (v/v, 7/3). The flow rate, column temperature, injection volume, and detection period were set to 0.7 mL min^{-1}, 30 °C, 10 μL, and 7.5 min, respectively. GLA was determined at a wavelength of 281 nm. Calculations of EE and LC were performed as below:

$$\text{EE (\%)} = \text{encapsulated GLA/total amount of GLA} \times 100\%$$

$$\text{LC (\%)} = \text{encapsulated GLA/total mass of zein and SPI} \times 100\%$$

2.6 Colloidal stability of GLA-loaded Zein/SPI nanocomposite particles

2.6.1 Effect of pH. Following dilution, the pH of the as-prepared particle dispersions was adjusted using HCl or NaOH. To prevent the influence of ionic strength, pH values were adjusted using solely HCl or NaOH solution. After 24 h at room temperature, samples were taken to determine the average diameter and zeta potential.

2.6.2 Effect of ionic strength. The influence of ionic strength on dispersion stability was investigated by adding different amounts of NaCl to as-prepared particle dispersions. After 24 h, samples were taken to determine the average diameter and zeta potential.

2.6.3 Storage stability. The as-prepared particle dispersions were stored at room temperature, and changes in average diameter and PDI were monitored at regular intervals.

2.7 Stability evaluation of free and encapsulated GLA

2.7.1 Photostability. The free GLA (dissolved in 20% (w/w) aqueous solution of isosorbide dimethyl ether) and its encapsulated forms (ZG_{10} and ZSG_{10}) were subjected to UV radiation (24 W, 254 nm) at room temperature. Samples were collected every hour, for a total of seven times, to measure the GLA content using the aforementioned approach.

2.7.2 Temperature. Free GLA and encapsulated GLA (ZG_{10} and ZSG_{10}) were heated at 80 °C for 8 h. A sample was withdrawn every two hours, and the GLA content was determined using the procedure described above.

2.7.3 Storage stability. Samples were kept at 25 °C and taken out at 0, 7, 14, 21, and 30 days to determine the GLA content using the aforementioned method.

$$\text{GLA retention (\%)} = \text{concentration of GLA after treatment/initial concentration of GLA} \times 100\%$$

2.8 Antioxidant activity

To comprehensively evaluate the antioxidant activity, two methods were employed: the ABTS radical scavenging assay and the ferric reducing antioxidant power (FRAP) assay. To produce ABTS radical cations ($ABTS^{\bullet+}$), a $K_2S_2O_8$ solution (4.9 mM) and an ABTS solution (7.0 mM) were reacted overnight in the dark. The resultant solution was diluted until the absorbance of the working solution was 0.70–0.80 (at 734 nm). In each experiment, the test sample (40 μL) was combined with the $ABTS^{\bullet+}$ working solution (160 μL). After 15 min of vibration in a dark environment, the absorbance (734 nm) was measured on a 96-well microplate reader. The equation for calculating $ABTS^{\bullet+}$ scavenging activity is as follows:

$$ABTS^{\bullet+}\text{ clearing activity (\%)} = [1 - (A_S - A_B)/A_C] \times 100\%$$

where A_C is the absorbance of the working solution with water (40 μL), A_S is the absorbance of the working solution with the sample (40 μL), A_B is the absorbance of 40 μL sample with 160 μL of water.

In parallel, the TPTZ working solution was prepared freshly by mixing 10 mM TPTZ (dissolved in 40 mM HCl), 20 mM $FeCl_3$, and 0.3 M sodium acetate buffer (pH 3.6) in a volume ratio of 1 : 1 : 10. A volume of 100 μL of each sample was added to 3 mL of TPTZ working solution and incubated at 37 °C for 15 min. Then, 200 μL of the reaction mixture was transferred to a

96-well microplate, and the absorbance was measured at 593 nm. The FRAP activity was quantified using a standard curve prepared with ascorbic acid solutions (10 to 1000 μM), and results were expressed as μM of ascorbic acid equivalent.

2.9 *In vitro* cytotoxicity assay

The biocompatibility of ZNPs, SPI and Zein/SPI$_{1:1}$ were evaluated using HaCaT and NCM-460 cells. Cells were seeded in 96-well plates at a given density (10 000 cells per well), and then incubated in an incubator for 24 h (37 °C, 5% CO_2). The culture medium was then removed, and different concentrations of sample dispersions (100 μL) were added for another 24-hour incubation. After that, the particle dispersions were separated out and cells were washed with PBS, followed by the addition of CCK-8 working solution (100 μL). The plates were incubated at 37 °C for 1.5 h, and the absorbance at 450 nm was recorded. The CCK-8 working solution was composed of CCK-8 reagent and culture medium with a volume ratio of 1/9.

$$\text{Cell survival (\%)} = (A_S - A_B)/(A_C - A_B) \times 100\%$$

where A_C, A_S and A_B are the absorbance of the control group, the sample group, and the CCK-8 working solution, respectively.

2.10 *In vitro* release behavior

A dispersion (10 mL) of free GLA, ZSG_{10} or ZG_{10} was placed in a dialysis bag (Viskase, USA) with an M_w cutoff of 7000 Da and dialyzed against 100 mL release medium (10 mM PBS and 0.2% (w/w) Tween-80) at a pH of 7.4. The experiment was carried out in a shaker incubator (100 rpm) at 37 °C. At specified intervals, the release medium (200 μL) with released GLA was collected from the dialysis apparatus and replaced with an equivalent volume of fresh release medium. Released GLA was determined using the HPLC method.

Released GLA (%) = released GLA/total amount of GLA × 100%

2.11 Statistical analysis

Every experiment was carried out in triplicate. Data were displayed as mean ± standard deviation (SD). Statistical significance was assessed using one-way analysis of variance (ANOVA) followed by Tukey's *post-hoc* test, with $p < 0.05$ considered statistically significant.

3. Results and discussion

3.1 Formation and characterization of Zein/SPI nanocomposite particles

ZNPs can be easily made through anti-solvent precipitation in aqueous ethanol by changing the ethanol concentration using water. In Fig. 1a, the average diameter of plain ZNPs prepared at a pH of 5 was around 87.44 nm with a positive zeta potential of about 25.94 mV (Fig. 1b). Interestingly, the addition of SPI during the anti-solvent process had a significant effect on the final physicochemical properties of the resulting particles. The average diameter of the resulting Zein/SPI nanocomposite particles was larger than that of ZNPs, suggesting that a complex between SPI and zein had formed. Furthermore, the zeta potential shifted from positive to negative, and gradually increased, and then remained constant when the mass ratio of zein to SPI further increased. The results could be explained by the isoelectric points of zein and SPI, which are approximately 5.9 and 3.3, respectively (Fig. 1c). At a pH of 5, therefore, zein and SPI had opposing charges. In addition, Zein/SPI nanocomposite particles were negatively charged, indicating their surface was dominated by SPI.[27]

Furthermore, at a mass ratio of 1 : 0.25, zein and SPI formed large aggregates, resulting in visible sediments (Fig. S1). Fig. 1b shows how the mass ratios of two different proteins were crucial for adjusting the surface charges of the resulting nanocomposite particles. An electrical equivalency could be established when the mass ratio of zein to SPI approaches 1 : 0.25. The charge magnitude of the nanocomposite particles was relatively low, leading to negligible electrostatic repulsion between them. This explains the high level of particle aggregation. As the amount of SPI increased, the average diameter of resulting Zein/SPI nanocomposite particles fell dramatically, and subsequently stabilized at around 250 nm. The minimum average diameter (234.64 nm) was found when the mass of zein was equal to SPI, which was almost 2.7 times larger than the average diameter of plain ZNPs. The zeta potential reached a relatively high level (−27.44 mV) around this mass ratio, similar to the zeta potential of SPI (Fig. 1b). It is widely known that a

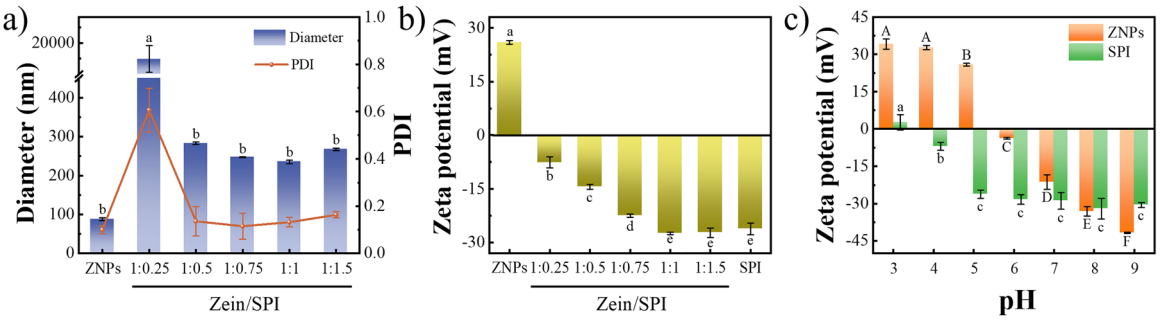

Fig. 1 Effect of Zein/SPI mass ratios on average diameter and PDI (a), zeta potential (b) of resulting nanocomposite particles, effect of pH on zeta potentials of ZNPs and SPI (c). Different letters represent significant differences ($p < 0.05$).

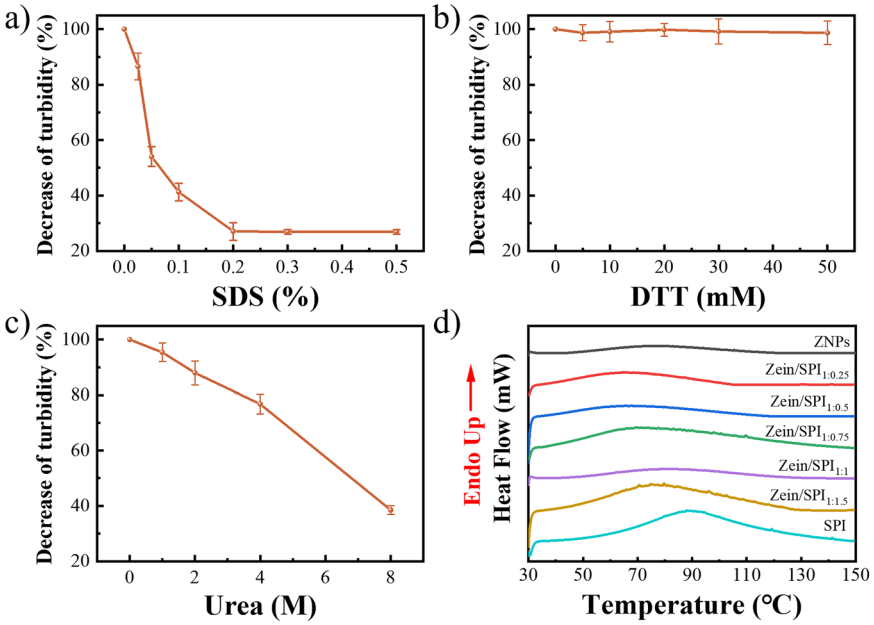

Fig. 2 Effect of the concentration of SDS (a), urea (b) and DTT (c) on the turbidity of aqueous dispersion of Zein/$SPI_{1:1}$. DSC thermograms of ZNPs, SPI, and various Zein/SPI nanocomposite particles (d).

particle dispersion is colloidally stable when the zeta potential approaches positive or negative 30 mV. Except for Zein/$SPI_{1:0.25}$, a PDI of less than 0.2 was observed for all these nanocomposite particles, a value that is indicative of a narrow size distribution.

Apart from electrostatic interaction, two distinct proteins are usually bound by hydrogen bonding and/or hydrophobic interaction. Fig. 2(a–c) shows that after treating the as-prepared aqueous dispersion of Zein/$SPI_{1:1}$ with SDS, urea, and DTT, the turbidity decreased to 26.81%, 38.46%, and 98.66%, respectively. DTT treatment reduced turbidity by less than 2%, indicating that it had little effect on the structure of colloidal particles. However, the large decreases in turbidity observed after post-treatment with urea and SDS indicated that hydrogen bonds coupled with hydrophobic interactions were the primary driving forces behind protein combination.[26,28] In short, when the pH is 5.0, zein is positively charged and SPI is negatively charged. They approach each other through electrostatic interaction, and as they get closer, hydrogen bonding and hydrophobic interactions become more active, thereby promoting the formation of stable nanocomposite particles.

To further verify the structural stability of the resulting nanocomposite particles, differential scanning calorimetry (DSC) was conducted (Fig. 2d). Both ZNPs and SPI exhibited endothermic transitions at approximately 77 and 89 °C, respectively, which can be attributed to the denaturation of the two proteins.[29,30] Interestingly, Zein/$SPI_{1:0.25}$ displayed a lower endothermic peak temperature (*ca.* 66 °C) compared to pure ZNPs, which was likely due to its loose internal structure.[31,32] As the SPI proportion increased, the endothermic transition gradually shifted toward higher temperatures, indicating enhanced thermal resistance.[31,32] This elevation in denaturation temperature reflects the formation of a more compact network, possibly due to the simultaneous action of electrostatic attraction, hydrogen bonding, and hydrophobic interactions. Therefore, combining the results of average diameter, zeta potential and stability, the Zein/SPI nanocomposite particles prepared at a mass ratio of zein to SPI of 1 : 1 (Zein/$SPI_{1:1}$) were selected for the following studies to further investigate their formation and application.

3.2 Preparation of GLA-loaded Zein/SPI nanocomposite particles (ZSG)

Fig. 3 and 4 show how GLA concentration affects the formation of ZSG. After adding GLA, the morphology of ZSG (Fig. 3) remained unchanged from that of Zein/$SPI_{1:1}$ nanocomposite particles. These nanoparticles had a spherical morphology suggesting that GLA was effectively encapsulated. As shown in Fig. 4, the average diameter and surface charge of ZSG were similar to those of the Zein/$SPI_{1:1}$ nanocomposite particles, with an average diameter of 224.61 to 206.77 nm and a zeta potential of −24.78 to −19.67 mV. The PDI was always less than 0.2, indicating that these nanoparticles had a narrow size distribution. These results suggested that adding GLA had little effect on the binding behavior of zein and SPI. Instead, the interactions between zein and SPI are likely to be the dominant factor in maintaining the morphology, average diameter, PDI, and zeta potential.

EE and LC are critical characteristics for determining if the designed delivery system is suitable for the intended use. Fig. 4c shows that, as GLA increased from 5 to 25 mg, the EE decreased while the LC increased. Previous research on paclitaxel and quercetagetin reported comparable results.[27,33] In addition, as shown in Fig. S2, all of the test particles with SPI

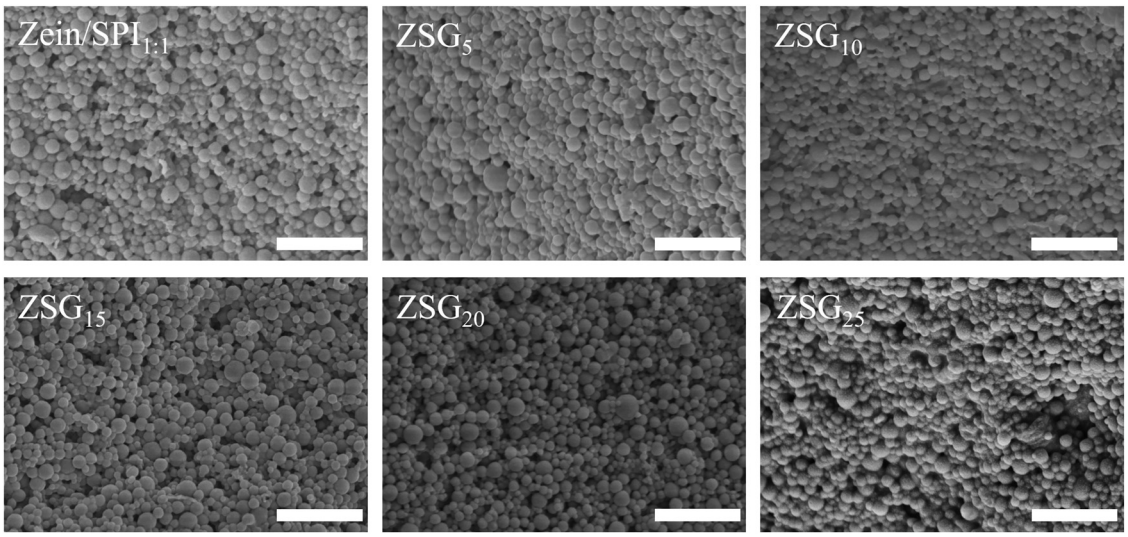

Fig. 3 SEM images of Zein/SPI$_{1:1}$ and ZSG prepared with different concentrations of GLA. Scale bars are 1 μm, magnification is ×30 000.

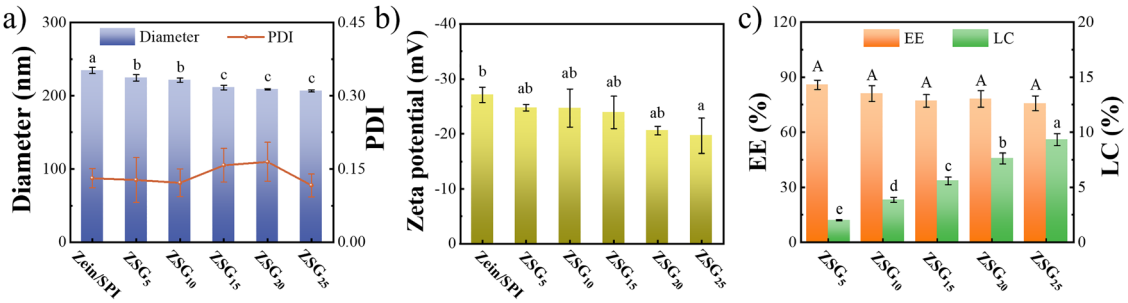

Fig. 4 Average diameter and PDI (a), zeta potential (b), EE and LC (c) of ZSG prepared with different concentrations of GLA. Different letters represent significant differences ($p < 0.05$).

incorporation had similar EE to those of the corresponding GLA-loaded ZNPs (ZG). This indicated that the presence of SPI did not interfere with the GLA incorporation into the zein core, and zein played a primary role in GLA encapsulation. On the other hand, as expected, ZSG had a lower LC than the corresponding ZG due to the increased overall weight of the nanoparticles after SPI incorporation. Overall, positively charged zein could be combined with negatively charged SPI to form a compact structure of nanocomposite particles with strong encapsulation ability. Therefore, Zein/SPI nanocomposite particles may serve as an ideal carrier with a high bioactive concentration and a high EE value. For example, when 10 mg of GLA was added, the EE and LC of ZSG$_{10}$ were around 81.07% and 3.85% respectively, while maintaining a small size, narrow size distribution, and relatively high zeta potential. Based on the above results, ZSG$_{10}$ was chosen for the following investigation.

3.3 Characterization of ZSG

The UV-vis spectrum of GLA in Fig. 5a shows a maximum absorption at 281 nm. Both ZNPs and SPI exhibited the characteristic absorption below 280 nm, while SPI also showed an obvious absorption at about 620 nm. The former was mainly owing to the distinctive absorption of tyrosine and tryptophan residues in the structures of the two proteins, whereas the latter could be attributed to the linear tetrapyrrole structure of phycocyanin in SPI.[25] As for Zein/SPI$_{1:1}$, it exhibited the distinctive absorptions of both ZNPs and SPI. Since the typical absorption wavelengths of GLA and ZNPs were similar, loading of GLA into Zein/SPI$_{1:1}$ resulted in no additional characteristic absorption. However, at around 280 nm, the ZSG$_{10}$ exhibited greater absorbance, indicating the GLA encapsulation in the Zein/SPI$_{1:1}$ was successful. Furthermore, on increasing the GLA concentration, the absorption of GLA-loaded nanocomposite particles at this wavelength increased (Fig. S3). This also suggested that the LC increased, corresponding with the previous quantitative results.

Fluorescence spectroscopy was also employed to investigate the formation of ZSG and their intermolecular interactions. The fluorescence spectrum of ZNPs in Fig. 5b reveals a remarkable emission peak at about 309 nm. The location of this emission peak was related to the high tyrosine residue content and low tryptophan residue content.[34] The emission peaks of SPI were around 309, 345 and 440 nm, respectively. The fluorescence

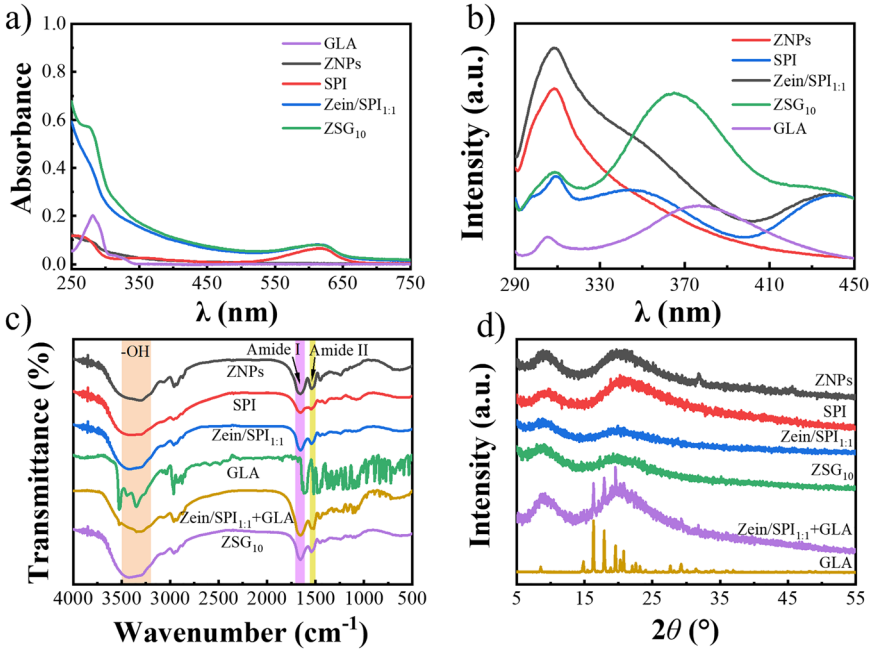

Fig. 5 UV-vis (a) and fluorescence spectra (b) of ZNPs, SPI, Zein/SPI$_{1:1}$ and ZSG$_{10}$ in water as well as GLA in ethanol. FTIR spectra (c) and XRD patterns (d) of ZNPs, SPI, Zein/SPI$_{1:1}$, GLA, ZSG$_{10}$, Zein/SPI$_{1:1}$ + GLA (physical mixture of Zein/SPI$_{1:1}$ and GLA with mass ratio of 20 : 1).

emission signals at 309 and 345 nm represent the fluorescence signals of tyrosine and tryptophan residues in SPI, while 440 nm could be ascribed to nicotinamide adenine dinucleotide phosphate, a main photosynthetic product.[35] When zein was combined with SPI, the fluorescence intensity of the zein component at about 309 nm increased. This finding might stem from the formation of Zein/SPI nanocomposite particles. It prompts the zein molecule chains to unfold, thus exposing tyrosine residues that were hidden in the hydrophobic interior originally.[36]

Notably, the fluorescence intensity at 309 nm in ZSG$_{10}$ was lower than that in Zein/SPI$_{1:1}$. Furthermore, as shown in Fig. S4, increasing the loading amount of GLA caused the fluorescence intensity at 309 nm to gradually decrease. This decrease suggested that the tyrosine residues in ZSG were quenched after interacting with GLA, implying that it bound to the protein.[34] This phenomenon was consistent with previous reports that the binding of resveratrol or quercetagetin to zein led to fluorescence quenching of zein.[27,34] On the other hand, when GLA was encapsulated in ZSG, its fluorescence intensity considerably increased. Additionally, the maximum wavelength shifted from 376 to 365 nm. The increased fluorescence intensity and shift in the maximum emission wavelength could be due to GLA binding to the hydrophobic moieties of zein.[37]

In Fig. 5c, FTIR spectra show that ZNPs and SPI exhibit broad characteristic peaks at about 3303.6 and 3292.3, respectively. Previous reports attributed the bands between 3200 and 3500 cm^{-1} to hydroxyl stretching vibrations.[38] Other peak areas belonged to amide I (stretching vibration of carbonyl group) and amide II (bending vibration of N–H coupled with stretching vibration of C–N). These two bands of ZNPs appeared at 1653.7 (amide I) and 1540.8 (amide II) cm^{-1}, respectively. SPI had two characteristic amide peaks, amide I and amide II, at 1653.5 and 1544.5 cm^{-1}, respectively. As for Zein/SPI$_{1:1}$, the hydroxyl stretching vibrations, as well as amide I and amide II, were slightly displaced to 3304.1, 1653.6, and 1541.0 cm^{-1}, respectively. The former suggested that a hydrogen bond was present between SPI and zein, whereas the latter might have been caused by the hydrophobic and electrostatic interactions.[20,39] These results corresponded to the driving force analysis in section 3.1. The GLA spectrum showed no peak in the carbonyl region, which was a characteristic of protein adsorption. When compared to the spectrum of GLA, most of the characteristic peaks of GLA disappeared in the spectrum of ZSG$_{10}$; however, practically most of these peaks remained in the spectrum of their physical mixtures. This result may be due to the limited bending and stretching of GLA's bonds when incorporated into the nanoparticles.[40] Furthermore, the disappearance of these peaks was mainly connected with the vibrations of aromatic rings and inter-ring aliphatic chains.[41] These changes could indicate that GLA was encapsulated in the nanocomposite particles and that the primary structure of proteins was not changed by GLA loading.

Fig. 5d shows that the X-ray diffraction patterns of a series of samples differed significantly. ZNPs and SPI exhibited two flat peaks at 2θ of 9.3°/20.3° and 9.3°/20.7°, respectively.[42,43] This demonstrated the amorphous structure of the two proteins. The peak intensity and position of Zein/SPI$_{1:1}$ differed from those of individual ZNPs and SPI. These results suggested that intermolecular interactions occurred between zein and SPI.[44] These interactions can slightly modify molecular structure, resulting in small but discernible diffraction changes.[45] In

contrast, the diffraction peaks of GLA were sharp and distinct, indicating a highly crystalline structure. In contrast to GLA alone, the diffraction peaks of GLA in the ZSG_{10} nearly totally disappeared. However, the distinct XRD signals of GLA were clearly observed in the physical mixture of Zein/$SPI_{1:1}$ and GLA. This finding revealed that GLA was encapsulated in the nanocomposite particles and well-dispersed within the carrier proteins, implying that the encapsulated GLA transitioned from a crystalline to an amorphous state. These results indicated not only the formation of GLA-loaded nanocomposite particles, but also the presence of molecular interactions between GLA and the carrier proteins.[27]

3.4 Colloidal stability of ZSG

Nanoparticles are expected to be exposed to various pH levels during storage and applications, so it is crucial to assess the colloidal stability of ZSG under varied pH situations. As shown in Fig. 6a, the dispersion stability of ZSG_{10} was strongly related to the pH levels. They remained stable at pH levels ranging from 5 to 9, with a relatively small average diameter of around 210 nm. In contrast, ZG_{10} aggregated noticeably at a neutral pH level (Fig. S5). Fig. 1c depicts ZNPs with an isoelectric point at pH 5.9 and SPI at pH 3.3. And the ZSG_{10} had a similar isoelectric point at around 3.7 to SPI, as a result of their outer layer being dominated by SPI. Therefore, the ZSG_{10} did not aggregate between pH 6 and 7, as ZG_{10} do, indicating that SPI adsorption effectively stabilized the zein core.[44] It provided electrostatic and steric repulsion, which resisted the van der Waals forces and hydrophobic attraction.[39] Furthermore, when the pH approached the isoelectric point of ZSG_{10}, aggregation occurred at pH 3 and 4.

Salt tolerance of delivery systems is another key indicator of colloidal stability. As illustrated in Fig. 6b, the size of nanoparticles increases in proportion to the concentration of NaCl. They were relatively stable at salt concentrations below 50 mM, but displayed considerable aggregation at 50 mM, resulting in a large increase in particle diameter. However, salt stability was shown to be superior to that of ZG_{10}. Destabilization of ZG_{10} happened when the concentration of NaCl reached up to 10 mM (Fig. S6). As salt concentration increased, the zeta potential of nanoparticles decreased. The adsorption of Na^+ and Cl^- on the surface of nanoparticles resulted in an electrostatic shielding effect, which reduced electrostatic repulsion between nanoparticles and explained the positive linear connection between the particle size and ionic strength.[46] Chen *et al.* also found that adding salt (0–50 mM) caused the anionic polymeric stabilizer (gum Arabic) to detach from ZNPs, resulting in aggregation.[47] These results suggest that ZSG may have limited applications in food, cosmetic, and pharmaceutical products with high ionic strengths, even though SPI improves their stability.

The long-term storage stability of ZSG is essential for its practical application as a delivery system. The ZSG_{10} was stored at room temperature for 4 weeks. Fig. 6c depicts the changes in average diameter and PDI for ZSG_{10}. Throughout the storage period, ZSG_{10} exhibited good storage stability, as evidenced by the negligible change in all measurements. The average diameter stayed as when initially prepared, with a narrow size distribution (PDI less than 0.2). This finding indicated that the prepared ZSG_{10} had excellent colloidal stability over time, which was due to the steric and electrostatic repulsion provided by SPI.

3.5 Protection of encapsulated GLA

The degradation resistance of GLA encapsulated in Zein/SPI nanocomposite particles was assessed after UV irradiation, heating, and long-term storage, with free GLA and GLA encapsulated in ZNPs serving as control groups. Fig. 7a shows that the GLA retention rate in the three systems decreased with UV irradiation. This phenomenon is caused by the structural characteristics of GLA molecules, which include unsaturated bonds that are easily broken when exposed to UV light, resulting in molecule breakdown.[48] Of the three, free GLA showed the most apparent drop. Its retention rate decreased to 86.72% after 6 h. The retention rate of GLA encapsulated in ZSG_{10} and ZG_{10} was 96.64% and 92.16%, respectively. The enhanced UV resistance of encapsulated GLA was attributed to the aromatic amino acid residues of zein, which helped absorb UV light.[49] ZSG_{10} is more resistant to UV light than ZG_{10}, possibly because of the presence of additional SPI coating on the nanoparticle surface. This acts as a physical barrier that partially absorbs UV light, thereby attenuating the radiation reaching the encapsulated GLA.[21,25] As shown in Fig. 7b, when heated at 80 °C, the free GLA degraded severely. After 8 h, its retention rate was just 24.67%. Following encapsulation, the retention rates of GLA in ZSG_{10} and ZG_{10} were 95.10% and 90.99%, respectively. This

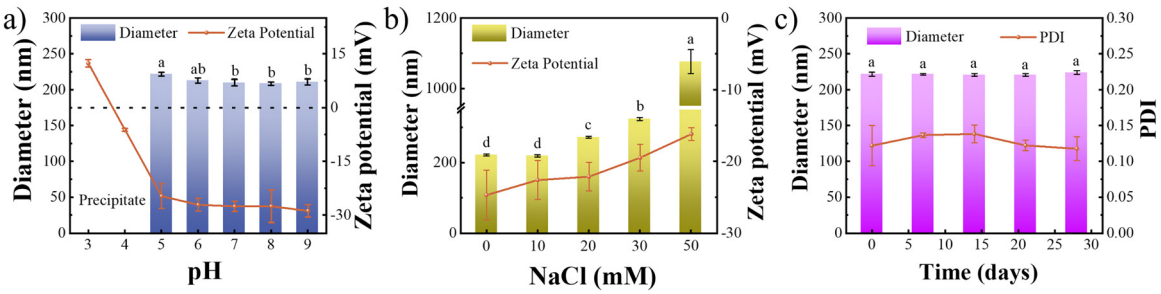

Fig. 6 Effect of pH (a), NaCl concentration (b), and storage time (c) on the average diameter, zeta potential, or PDI of ZSG_{10}. Different letters represent significant differences ($p < 0.05$).

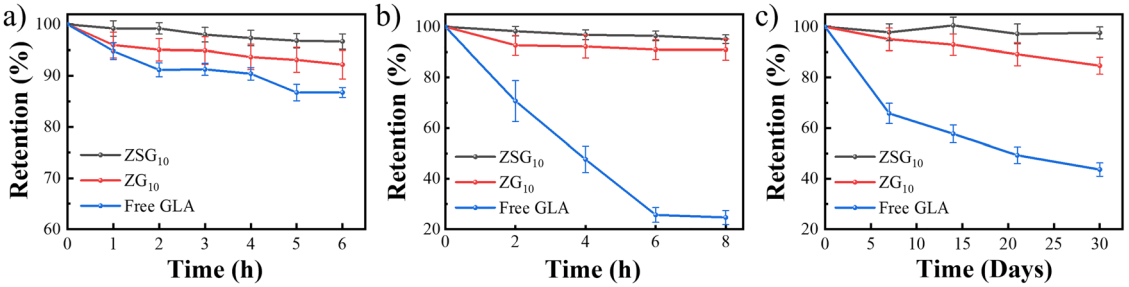

Fig. 7 Effects of UV irradiation (a), heating (80 °C) (b), and storage time (c) on the retention rate of GLA encapsulated in ZG_{10} and ZSG_{10} as well as free GLA.

indicates that carrier proteins act as a thermal barrier or GLA structure stabilizer, shielding GLA from high temperature and inhibiting heat-induced degradation. As for long-term storage (Fig. 7c), free GLA also did not do well. After 30 d, the retention rate dropped to 43.65%. This may be due to a gradual chemical reaction between GLA and environmental factors such as oxygen and moisture during storage.[48] However, carrier proteins continued to give excellent protection. ZSG_{10} retained 97.57% of GLA, while ZG_{10} retained 84.67% after 30 d.

3.6 Antioxidant properties of encapsulated GLA

The $ABTS^{\bullet+}$ clearing experiment was first employed to evaluate the antioxidant activity of the samples. As displayed in Fig. 8a, the SPI had a greater clearance rate for $ABTS^{\bullet+}$ than ZNPs did, which can be ascribed to the different amino acid residues and the presence of phycocyanin with a high antioxidant activity in SPI. GLA has excellent antioxidant properties because of the presence of phenolic hydroxyl groups.[50] However, GLA dispersed in water shows low free radical scavenging activity, which could be due to its poor water solubility which makes it difficult to dissolve in water. Interestingly, the antioxidant activity of GLA improves dramatically after encapsulation, implying that encapsulating GLA in nanoparticles is an efficient strategy to increase its antioxidant activity. This could be because of the improved dispersion of GLA in water, increasing its chances of contacting free radicals. Several studies have reported similar phenomena.[39,51] In addition, compared to ZNPs as the carrier, GLA encapsulated in Zein/SPI nanocomposite particles has better antioxidant activity. This could be because SPI has a higher antioxidant capacity than ZNPs.

To further validate the results obtained from the above, the FRAP test was conducted. The FRAP assay evaluates the electron-donating ability of antioxidants, providing complementary information on their overall reducing potential. As shown in Fig. 8b, the FRAP results exhibited a trend consistent with the $ABTS^{\bullet+}$ assay. SPI and GLA-loaded Zein/SPI nanocomposite particles showed markedly higher FRAP values than ZNPs or free GLA. These parallel results from two independent

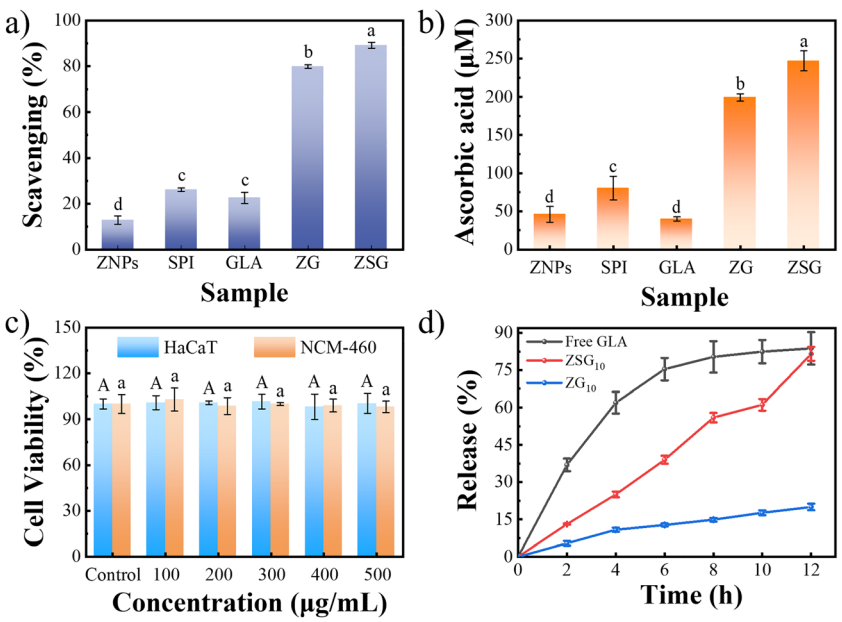

Fig. 8 $ABTS^{\bullet+}$ radical scavenging activity (a) and FRAP values (b) of ZNPs, SPI, GLA, ZG_{10} and ZSG_{10}. Cell viability of HaCaT and NCM-460 cells treated with different concentrations of Zein/$SPI_{1:1}$ (c). *In vitro* release profiles of GLA in free GLA and encapsulated in ZSG_{10} and ZG_{10} (d). Different letters represent significant differences ($p < 0.05$).

methods demonstrate that SPI possesses intrinsic antioxidant activity and that integration within Zein/SPI nanocomposite particles effectively amplifies the antioxidant performance of GLA.

3.7 *In vitro* cytotoxicity assay

Cytotoxicity testing is a common approach for evaluating the safety of nanomaterials. Here human immortalized epidermal cells (HaCaT) and normal human colon epithelial cells (NCM-460) were used as models to assess the safety of Zein/$SPI_{1:1}$ nanocomposite particles on skin and digestive tract, respectively. Fig. 8c shows the cell viability after incubating Zein/$SPI_{1:1}$ nanocomposite particles with two types of cells for 24 h. After incubation with various concentrations of protein for 24 h, HaCaT and NCM-460 cells all showed above 90% cell viability. This result indicated that Zein/$SPI_{1:1}$ nanocomposite particles have good biocompatibility. This is because zein and SPI are both biocompatible (Fig. S7) and there are no chemical reactions between them.

3.8 *In vitro* release of encapsulated GLA

Fig. 8d depicts the *in vitro* release characteristics of free GLA and its encapsulated forms in ZG and ZSG. Free GLA had a fast release rate, reaching 75.41% in just 6 h. In contrast to free GLA, both ZSG_{10} and ZG_{10} exhibited slow and sustained release profiles. Specifically, the release of GLA from ZG_{10} was extremely slow, with only 20.00% released after 12 h. This is mostly due to the flocculation and sedimentation of ZG_{10} at neutral pH (Fig. S8), which hinders medium penetration and significantly limits GLA diffusion into the release medium. As a result, the GLA cannot be fully released, which may compromise its usefulness in practical applications. On the other hand, ZSG_{10} showed a distinct, gradual and continuous release behavior. It released 39.03% of GLA within 6 h and 81.55% overall within 12 h. Clearly, ZSG_{10} allowed for more controlled and sustained release of GLA than free GLA, and it can also release most of the encapsulated GLA when compared to ZG_{10}. This is because, unlike encapsulation in ZG, where the instability of nanoparticles easily leads to aggregation and hinders the release of GLA from the particle interior, the introduction of SPI not only allows ZSG to be more stably dispersed in the release medium, but the SPI attached to the surface of the zein core can also regulate the release of GLA. This demonstrated that Zein/SPI nanocomposite particles are a more stable and efficient release carrier for GLA, indicating increased potential for GLA delivery.

4. Conclusion

This study successfully prepared Zein/SPI nanocomposite particles using a simple anti-solvent precipitation method and used them to encapsulate GLA. The optimized nanoparticles were spherical in shape, with a particle size of 234.64 nm, a narrow size distribution (PDI, 0.13), and a negative surface charge of −27.44 mV. Electrostatic interaction, hydrogen bonding, and hydrophobic interaction all contributed to the formation of Zein/SPI nanocomposite particles. When GLA was added, the resultant GLA-loaded Zein/SPI nanocomposite particles showed high EE and LC. Moreover, when GLA concentration increased, EE decreased while the LC increased. These nanocomposite particles (*e.g.*, ZSG_{10}) were found to be stable against aggregation over a pH range of 5 to 9, salt concentrations below 50 mM, and 28 days of storage at room temperature. They also effectively protected GLA from degradation against UV irradiation, high temperature, and long-term storage. In addition, GLA-loaded Zein/SPI nanocomposite particles significantly enhanced the antioxidant capacity, as indicated by increased $ABTS^{\bullet+}$ radical scavenging and FRAP values, compared to GLA dispersed in water. The protein-based carrier nanoparticles also exhibited good biocompatibility. *In vitro* release studies indicated that Zein/SPI nanocomposite particles could achieve the slow and sustained release of encapsulated GLA. Overall, Zein/SPI nanocomposite particles show great promise as delivery systems for hydrophobic bioactives in the food, cosmetic, and pharmaceutical industries.

Author contributions

Jie Mei: investigation, methodology, formal analysis and data curation. Chen Li: investigation and formal analysis. Beizhe Chang: data curation. Xiaomin Li: investigation. Yunxing Li: writing – review and editing, supervision and funding acquisition. Bingtian Zhao: supervision. Cheng Yang: conceptualization, supervision and project administration. To Ngai: conceptualization, supervision, writing – review and editing.

Conflicts of interest

There are no conflicts to declare.

Data availability

The data supporting this article have been included as part of the supplementary information (SI). Supplementary information is available. See DOI: https://doi.org/10.1039/d5sm00953g.

Acknowledgements

This work was supported by the National Natural Science Foundation of China (No. 22272064).

Notes and references

1 Z. Chen, T. Hu, R. Wang, B. Huang, L. Tu, G. Wang, C. Li, B. Dong, Z. Wang and W. Hu, *Adv. Healthcare Mater.*, 2023, **13**, 2302470.
2 S. Li, Y. Wang, M. Wu, M. H. Younis, A. P. Olson, T. E. Barnhart, J. W. Engle, X. Zhu and W. Cai, *Adv. Mater.*, 2022, **34**, 2204976.

3 L. Cheng, J. Xu, A. Wang, S. Hou and A. Li, *Colloids Surf., B*, 2025, **255**, 114979.
4 P. Liang, Y. Hu, Z. Wang, Y. Guo, H. Chen, C. Jiang, Q. Zeng, C. Shen, Y. Wu, L. Liu, Y. Yi, H. Zhu, Z. Yang and Q. Liu, *CrystEngComm*, 2023, **25**, 6252–6265.
5 Y. Fan, Q. Han, H. Li, X. Cai, B. Dyett, R. Qiao, C. J. Drummond, S. H. Thang and J. Zhai, *Adv. Sci.*, 2025, e07209.
6 H. Rostamabadi, S. R. Falsafi, M. M. Rostamabadi, E. Assadpour and S. M. Jafari, *Adv. Colloid Interface Sci.*, 2021, **290**, 102384.
7 K. Ulbrich, K. Holá, V. Šubr, A. Bakandritsos, J. Tuček and R. Zbořil, *Chem. Rev.*, 2016, **116**, 5338–5431.
8 M. Hadidi, C. Tan, E. Assadpour, M. S. Kharazmi and S. M. Jafari, *J. Controlled Release*, 2023, **355**, 327–342.
9 T. Chen, C. Li, Y. Li, X. Yi, R. Wang, S. M.-Y. Lee and Y. Zheng, *ACS Appl. Mater. Interfaces*, 2017, **9**, 9516–9527.
10 A. R. Patel and K. P. Velikov, *Curr. Opin. Colloid Interface Sci.*, 2014, **19**, 450–458.
11 J. W. J. de Folter, M. W. M. van Ruijven and K. P. Velikov, *Soft Matter*, 2012, **8**, 6807.
12 P. K. Pandey, P. Kaushik, K. Rawat, V. K. Aswal and H. B. Bohidar, *Soft Matter*, 2017, **13**, 6784–6791.
13 W. Jiang, H. Jiang, W. Liu, X. Guan, Y. Li, C. Yang and T. Ngai, *Acta Phys. Chim. Sin.*, 2023, **39**, 2301041.
14 A. Patel, Y. C. Hu, J. K. Tiwari and K. P. Velikov, *Soft Matter*, 2010, **6**, 6192–6199.
15 P. H. L. Tran, W. Duan, B.-J. Lee and T. T. D. Tran, *Int. J. Pharm.*, 2019, **566**, 557–564.
16 M. D. Leonida, I. Kumar, A. Benzecry, J. Song, C. Jean and S. Belbekhouche, *ACS Biomater. Sci. Eng.*, 2023, **9**, 6165–6174.
17 H. Hou, D. Zhang, J. Zeng, L. Zhou, Z. Wang, M. Yao, J. Ren, N. Hu and Y. Wang, *Langmuir*, 2019, **35**, 3710–3716.
18 J. Feng, Y. Zhang, S. A. McManus, R. Qian, K. D. Ristroph, H. Ramachandruni, K. Gong, C. E. White, A. Rawal and R. K. Prud'homme, *Soft Matter*, 2019, **15**, 2400–2410.
19 A. R. Patel, E. C. M. Bouwens and K. P. Velikov, *J. Agric. Food Chem.*, 2010, **58**, 12497–12503.
20 D. Zhang, F. Jiang, J. Ling, X. Ouyang and Y. Wang, *Colloids Surf., B*, 2021, **204**, 111827.
21 J. Ding, Y. Li, Q. Wang, L. Chen, Y. Mao, J. Mei, C. Yang and Y. Sun, *Food Hydrocolloids*, 2023, **137**, 108369.
22 R. Liu, Y. Li, C. Zhou and M. Tan, *Food Funct.*, 2023, **14**, 4254–4266.
23 L. Böcker, P. Bertsch, D. Wenner, S. Teixeira, J. Bergfreund, S. Eder, P. Fischer and A. Mathys, *J. Colloid Interface Sci.*, 2021, **584**, 344–353.
24 M. P. Spínola, A. R. Mendes and J. A. M. Prates, *Foods*, 2024, **13**, 3656.
25 T. Xu, L. Yan, C. Liu and L. Zheng, *Food Chem.*, 2025, **464**, 141729.
26 Y. P. Xie, Y. J. Wang, Y. Sun, J. Y. Yao, T. Li, X. H. Zhang, Y. Wang, J. Huang, B. H. Xia, S. B. Wang and W. F. Dong, *Colloids Surf., A*, 2024, **686**, 133384.
27 C. Sun, L. Dai and Y. Gao, *Biomacromolecules*, 2016, **17**, 3973–3985.
28 A. Akbari and J. P. Wu, *Food Hydrocolloids*, 2016, **54**, 107–118.
29 C. Sun, L. Dai, X. He, F. Liu, F. Yuan and Y. Gao, *Food Hydrocolloids*, 2016, **58**, 11–19.
30 J. Zhang, C. Wen, H. Zhang, M. Zandile, X. Luo, Y. Duan and H. Ma, *Int. J. Food Prop.*, 2018, **21**, 128–138.
31 S. Chen, C. Sun, Y. Wang, Y. Han, L. Dai, A. Abliz and Y. Gao, *J. Agric. Food Chem.*, 2018, **66**, 7441–7450.
32 Q. Liu, X. Chang, Y. Shan, F. Fu and S. Ding, *J. Sci. Food Agric.*, 2020, **101**, 3630–3643.
33 H. Liang, Q. Huang, B. Zhou, L. He, L. Lin, Y. An, Y. Li, S. Liu, Y. Chen and B. Li, *J. Mater. Chem. B*, 2015, **3**, 3242–3253.
34 I. J. Joye, G. Davidov-Pardo, R. D. Ludescher and D. J. McClements, *Food Chem.*, 2015, **185**, 261–267.
35 S. Benelhadj, A. Gharsallaoui, P. Degraeve, H. Attia and D. Ghorbel, *Food Chem.*, 2016, **194**, 1056–1063.
36 M. Liao, R. Zhang, Y. Zhou, D. Xu, Y. Han, F. Liu, J. Su and S. Chen, *Food Hydrocolloids*, 2023, **142**, 108774.
37 Q. G. Liu, Y. Q. Jing, C. P. Han, H. Zhang and Y. M. Tian, *Food Hydrocolloids*, 2019, **93**, 432–442.
38 M. A. Cerqueira, B. W. S. Souza, J. A. Teixeira and A. A. Vicente, *Food Hydrocolloids*, 2012, **27**, 175–184.
39 A. Mariano, Y. O. Li, H. Singh, D. J. McClements and G. Davidov-Pardo, *Food Hydrocolloids*, 2024, **153**, 110024.
40 Y. Wei, Z. Yu, K. Lin, C. Sun, L. Dai, S. Yang, L. Mao, F. Yuan and Y. Gao, *Food Hydrocolloids*, 2019, **95**, 336–348.
41 K. Hu, X. Huang, Y. Gao, X. Huang, H. Xiao and D. J. McClements, *Food Chem.*, 2015, **182**, 275–281.
42 Y. C. Luo, T. T. Y. Wang, Z. Teng, P. Chen, J. H. Sun and Q. Wang, *Food Chem.*, 2013, **139**, 224–230.
43 Y. Ladjal-Ettoumi, M. Hamadi, L. Hadjer Douik, Z. Cherifi and A. Nazir, *Algal Res.*, 2024, **81**, 103561.
44 H. Li, D. Wang, C. Liu, J. Zhu, M. Fan, X. Sun, T. Wang, Y. Xu and Y. Cao, *Food Hydrocolloids*, 2019, **87**, 342–351.
45 X. Zhan, L. Dai, L. Zhang and Y. Gao, *Food Hydrocolloids*, 2020, **106**, 105839.
46 Y. Wei, C. Li, L. Dai, L. Zhang, J. F. Liu, L. K. Mao, F. Yuan and Y. X. Gao, *Food Funct.*, 2020, **11**, 9973–9983.
47 H. Q. Chen and Q. X. Zhong, *Food Hydrocolloids*, 2015, **43**, 593–602.
48 J. Chen, Q. Fang, S. Liu, G. Yang and Y. Gao, *J. Photochem. Photobiol., A*, 2017, **339**, 12–18.
49 F. Z. Zhou, X. N. Huang, Z. L. Wu, S. W. Yin, J. H. Zhu, C. H. Tang and X. Q. Yang, *J. Agric. Food Chem.*, 2018, **66**, 11113–11123.
50 Y. Wei, J. Zhang, Y. Zhou, W. Bei, Y. Li, Q. Yuan and H. Liang, *Carbohydr. Polym.*, 2017, **159**, 152–160.
51 Y. Li, S. Lv, Y. Liu, S. Deng and G. Liu, *Ind. Crops Prod.*, 2024, **211**, 118229.

